The Astrophysical Journal Letters, 872:L9 (11pp), 2019 February 10 https://doi.org/10.3847/2041-8213/ab01e1

Diverse Variability of O and B Stars Revealed from 2-minute Cadence Light Curves in Sectors 1 and 2 of the *TESS* Mission: Selection of an Asteroseismic Sample

May G. Pedersen[1], Sowgata Chowdhury[2], Cole Johnston[1], Dominic M. Bowman[1], Conny Aerts[1,3], Gerald Handler[2], Peter De Cat[4], Coralie Neiner[5], Alexandre David-Uraz[6], Derek Buzasi[7], Andrew Tkachenko[1], Sergio Simón-Díaz[8], Ehsan Moravveji[1], James Sikora[9], Giovanni M. Mirouh[10], Catherine C. Lovekin[11], Matteo Cantiello[12,13], Jadwiga Daszyńska-Daszkiewicz[14], Andrzej Pigulski[14], Roland K. Vanderspek[15], and George R. Ricker[15]
[1] Instituut voor Sterrenkunde, KU Leuven, Celestijnenlaan 200D, B-3001 Leuven, Belgium; maygade.pedersen@kuleuven.be
[2] Nicolaus Copernicus Astronomical Center, Bartycka 18, 00-716 Warszawa, Poland
[3] Department of Astrophysics, IMAPP, Radboud University Nijmegen, P.O. Box 9010, NL-6500 GL Nijmegen, The Netherlands
[4] Royal Observatory of Belgium, Ringlaan 3, B-1180 Brussel, Belgium
[5] LESIA, Paris Observatory, PSL University, CNRS, Sorbonne Université, Univ. Paris Diderot, Sorbonne Paris Cité, 5 place Jules Janssen, F-92195 Meudon, France
[6] Department of Physics and Astronomy, University of Delaware, Newark, DE 19716, USA
[7] Dept. of Chemistry & Physics, Florida Gulf Coast University, 10501 FGCU Boulevard South, Fort Myers, FL 33965 USA
[8] Instituto de Astrofísica de Canarias, E-38200 La Laguna, Tenerife, Spain
[9] Department of Physics, Engineering Physics and Astronomy, Queens University, Kingston, ON K7L 3N6, Canada
[10] Astrophysics Research Group, Faculty of Engineering and Physical Sciences, University of Surrey, Guildford GU2 7XH, UK
[11] Physics Department, Mount Allison University, Sackville, NB, E4L 1C6, Canada
[12] Center for Computational Astrophysics, Flatiron Institute, 162 5th Avenue, New York, NY 10010, USA
[13] Department of Astrophysical Sciences, Princeton University, Princeton, NJ 08544, USA
[14] Instytut Astronomiczny, Uniwersytet Wrocławski, Kopernika 11, 51-611 Wrocław, Poland
[15] Department of Physics, and Kavli Institute for Astrophysics and Space Research, Massachusetts Institute of Technology, Cambridge, MA 02139, USA
Received 2019 January 5; revised 2019 January 18; accepted 2019 January 22; published 2019 February 8

Abstract

Uncertainties in stellar structure and evolution theory are largest for stars undergoing core convection on the main sequence. A powerful way to calibrate the free parameters used in the theory of stellar interiors is asteroseismology, which provides direct measurements of angular momentum and element transport. We report the detection and classification of new variable O and B stars using high-precision short-cadence (2 minutes) photometric observations assembled by the *Transiting Exoplanet Survey Satellite* (*TESS*). In our sample of 154 O and B stars, we detect a high percentage (90%) of variability. Among these we find 23 multiperiodic pulsators, 6 eclipsing binaries, 21 rotational variables, and 25 stars with stochastic low-frequency variability. Several additional variables overlap between these categories. Our study of O and B stars not only demonstrates the high data quality achieved by *TESS* for optimal studies of the variability of the most massive stars in the universe, but also represents the first step toward the selection and composition of a large sample of O and B pulsators with high potential for joint asteroseismic and spectroscopic modeling of their interior structure with unprecedented precision.

Key words: asteroseismology – binaries: general – stars: evolution – stars: massive – stars: oscillations (including pulsations) – stars: rotation

Supporting material: figure set, machine-readable table

1. Introduction

The variability of stars born with a mass $M \geqslant 3\,M_{\odot}$ is diverse in terms of periodicity (minutes to centuries) and amplitude (μmag to mag, see e.g., Aerts et al. 2010). Here, we are concerned with dwarfs, giants, and supergiants, of spectral type O or B. Such stars have a high binarity rate, a phenomenon that cannot be ignored when testing stellar evolution theory (Sana et al. 2014; Almeida et al. 2017; Schneider et al. 2018). Throughout their life, these stars are also subject to a strong variable radiation-driven wind (e.g., Lucy & Solomon 1970; Castor et al. 1975; Owocki & Rybicki 1984; Krtička & Feldmeier 2018).

Compared to other classes of variables, O stars have hardly been monitored with high-precision long-duration space photometry—see Table 3 in Buysschaert et al. (2015) for a summary of space photometric time-series studies of O stars, and more recent studies of their descendants including Pablo et al. (2017), Johnston et al. (2017), Buysschaert et al. (2017b), Aerts et al. (2018a), Simón-Díaz et al. (2018), and Ramiaramanantsoa et al. (2018b, 2018a). Aside from single and multiperiodic pulsational, binary, and rotational variability, these studies also revealed stochastic low-frequency variability. This observed phenomenon was interpreted in terms of internal gravity waves (IGWs) by Aerts & Rogers (2015). The observational signatures of IGWs have meanwhile been investigated systematically from *CoRoT* and *K2* data by Bowman et al. (2019a) and Bowman et al. (2019b), respectively. They offer an entirely new avenue of asteroseismic investigation by bridging 3D hydrodynamical simulations of stochastically excited waves and 1D theory of stellar interiors (Aerts et al. 2019, Figure 1).

Classical gravity-mode asteroseismology, i.e., forward modeling of the frequencies of coherent identified gravity modes (see Aerts et al. 2018b, for the methodology), has so far been limited to some 40 stars of spectral type B or F, covering the mass range $M \in [1.3, 8]\,M_{\odot}$ and rotation rates from almost zero up to 80% of critical breakup. This revealed the capacity of high-precision ($\sim$10%) mass estimation of single stars (see Moravveji et al. 2015, 2016; Szewczuk & Daszyńska-Daszkiewicz 2018, for B stars and Mombarg et al. (2019) for F stars), and of binaries (Kallinger et al. 2017; Johnston et al. 2019). So far, these asteroseismic studies

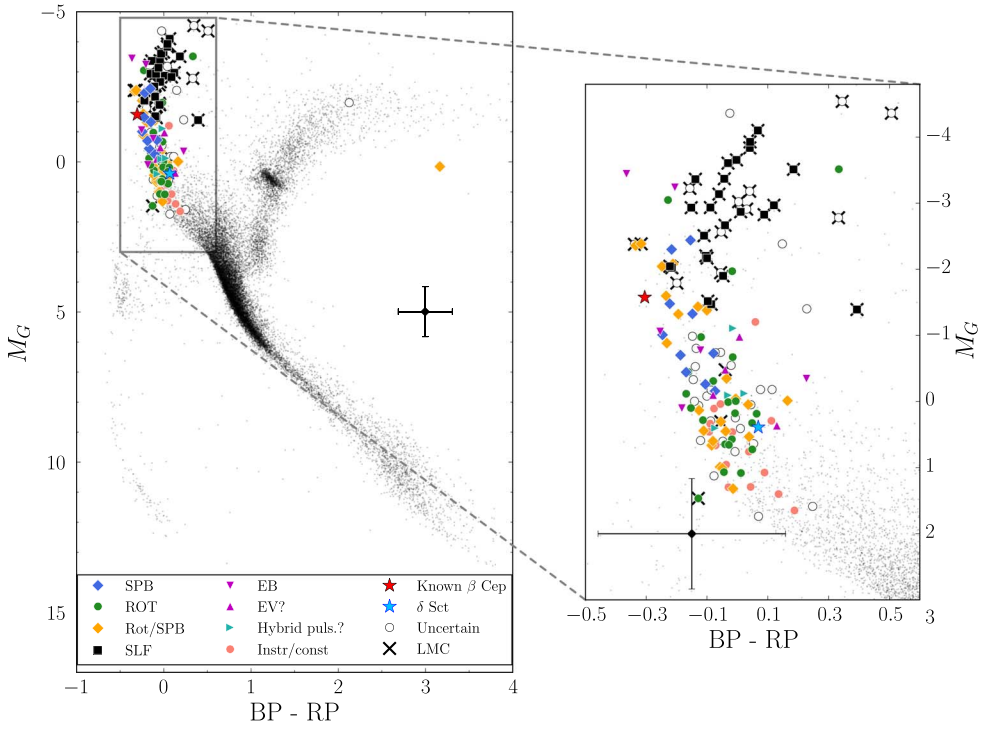

Figure 1. Classification results for O and B stars placed in a *Gaia* second data release (DR2) color–magnitude diagram (CMD). Black dots are the entire *Transiting Exoplanet Survey Satellite* (*TESS*) sector 1 and 2 short-cadence stars also observed by *Gaia*, and open black circles corresponds to uncertain classification. The labels in the legend correspond to the following types of variability: SLF = stochastic low-frequency signal; Instr/const = instrumental or constant; SPB = slowly pulsating B star; ROT = rotational modulation; ROT/SPB = rotational modulation and/or SPB; Hybrid puls.? = both p- and g-modes; EB = eclipsing binary; EV? = ellipsodal variable or rotational modulation; δ Sct = δ Scuti star. The error bar shows a typical 2σ-error on the position in the CMD, shown in both panels. Large Magellanic Cloud members are indicated by an $\times$ behind their variability symbol.

using space photometry revealed almost rigid rotation for the stars whose near-core ($\Omega_{\rm core}$) and envelope ($\Omega_{\rm env}$) rotation could be estimated, following the few earlier results of $\Omega_{\rm core}/\Omega_{\rm env} \in [1, 5]$ from ground-based asteroseismology of early-B stars (see Aerts 2015, for a summary). These asteroseismic findings challenge current angular momentum transport theories across the entire mass range (Aerts et al. 2019).

This Letter introduces our dedicated study to investigate single and binary O and B stars with the NASA *Transiting Exoplanet Survey Satellite* (*TESS*) mission (Ricker et al. 2015). In order to perform asteroseismology, one first needs to find suitable multiperiodic O and B pulsators. We achieve this by classifying the variability of 154 O and B stars observed in and proposed for short-cadence mode by the *TESS* Asteroseismic Science Consortium (TASC). We present our classification and selection strategy for the 2 minutes cadence light curves obtained in Sectors 1 and 2 of the *TESS* mission.

2. Method

2.1. TESS *Light Curve Extraction*

To study the variability of massive stars, we analyze a sample of 154 O and B stars observed by *TESS* with 2 minutes cadence, of which 40 are located in the Large Magellanic Cloud (LMC). These 154 stars were identified as O and B stars based on the spectral types provided in SIMBAD.[16] The data treated here were obtained by *TESS* in Sectors 1 (2018 July 25–August 22) and 2 (2018 August 23–September 20) and are publicly available via the Mikulski Archive for Space Telescopes (MAST).[17] The extracted time series are in the format of reduced Barycentric Julian Date (BJD—2457000) and stellar magnitudes, where the latter have been adjusted to show variability around zero by subtracting the mean. Where necessary, we performed detrending of long-term instrumental effects by means of subtracting a linear or low-order polynomial fit.

2.2. *Classification Procedure*

We calculated amplitude spectra of all light curves using discrete Fourier transforms (DFT) following the method by Kurtz (1985). We used an oversampling factor of 10 to ensure that all frequency peaks in the DFT are adequately sampled. The 2 minutes cadence of *TESS* results in a Nyquist frequency of 360 day^{-1}, which is sufficiently high enough to avoid a bias when extracting significant frequencies using iterative prewhitening. Amplitude suppression of variability in time series is negligible within the frequency range of interest for such high sampling (Bowman 2017). Based on visual inspection of the light curves and amplitude spectra by several of the authors independently, we provide the variability classification of all 154 O and B stars in Table 1 in Appendix A. We also report the number of available échelle spectra in the public ESO archive[18] for each of the stars and the instrument used for the observations. This information is relevant for future studies of these 154 O and B stars. Figures of the light curves and amplitude spectra are made available electronically in Appendix B.

[16] http://simbad.u-strasbg.fr/simbad/

[17] http://archive.stsci.edu/tess/all_products.html

[18] http://archive.eso.org/eso/eso_archive_main.html

2.3. Gaia *Color–Magnitude Diagram (CMD)*

Asteroseismic modeling of stars with coherent oscillation modes can be optimally performed if at least one additional global stellar parameter (aside from the identified oscillation frequencies) can be measured with high precision. The availability of such an independent measurement helps to break degeneracies among the global and local stellar model parameters to be estimated (e.g., Moravveji et al. 2015, their Figures 5 and B.1). A model-independent mass from binarity (Johnston et al. 2019) or a high-precision (10%) spectroscopic estimate of the effective temperature (Mombarg et al., 2019) have been used to break degeneracies. Another useful quantity is a star's luminosity (M. G. Pedersen et al. 2019, in preparation).

With this in mind, and to check the SIMBAD spectral types that went into the selection of our sample, we used *Gaia* second data release (DR2) photometry (Gaia Collaboration et al. 2018a) to place all sample stars in a CMD (Figure 1). Each star was color-coded by its dominant variability type. The apparent *Gaia* *G*-band magnitudes were converted to absolute magnitudes M_G using the *Gaia* DR2 distances from Bailer-Jones et al. (2018). The colors were derived from the apparent *Gaia* BP and RP band magnitudes. All other stars observed in 2 minutes cadence by *TESS* in Sectors 1 and 2 with *Gaia* DR2 data available (20,883 out of the 24,816 *TESS* targets) were included as black dots. Using the same approach as in Gaia Collaboration et al. (2018b), the position of the stars in Figure 1 have not been corrected for reddening or extinction, but we show a typical 2σ error bar for the positioning of the stars in the CMD. Two stars (TIC 197641601 = HD 207971 and TIC 354671857 = HD 14228) are outliers in the CMD (at BP–RP > 2). Although these stars are B stars, they are very bright ($V = 3.01$ and 3.57, respectively), which explains the discrepant *Gaia* photometry.

The 151 out of 154 stars in our sample observed with *Gaia* shown in Figure 1 constitute the first sample of variable O and B stars monitored at high cadence in high-precision space photometry, after the *K2* sample monitored at 30 minutes cadence in Bowman et al. (2019b). These two samples, along with future ones assembled by the *TESS* mission, will reveal numerous O and B stars suitable for asteroseismic modeling. Such modeling requires a frequency precision better than 0.001 day^{-1} and pulsation mode identification for tens of modes (Aerts et al. 2018b). In this way, we will extend the large *Kepler* samples of low-mass and intermediate-mass pulsators with an estimation of their interior rotation profile discussed in Aerts et al. (2019) to higher masses. The interior rotation and chemical mixing profiles will hence be calibrated asteroseismically for large samples of massive stars that will eventually explode as supernovae.

3. Results

It is not possible to discuss each star in the sample individually. Here we focus on the binarity and pulsational properties, and briefly discuss the detection of rotational and/or magnetic properties of the sample. Out of 154 stars, 41 show clear variability in their light curves but their nature could not yet be uniquely identified. These stars are marked by open black circles in Figure 1.

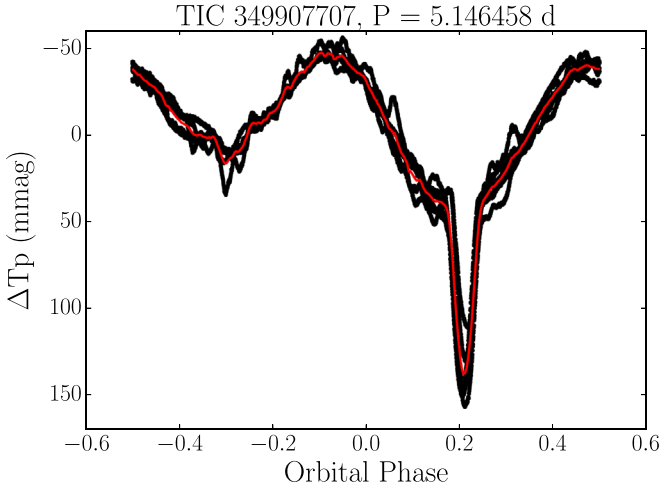

Figure 2. Phase-folded light curve (black) of the known eclipsing binary HD 61644, showing the signature of pulsations. The red line shows the binned phase curve.

3.1. Eclipsing Binaries (EBs)

EBs hold the potential to provide model-independent distance, radius, and mass estimates and are crucial calibrators for stellar evolution theory (see Torres et al. 2010, for a review). Unfortunately, the number of O and B stars in EBs observed with high-precision space photometry remains small compared to the thousands of binaries with low-mass components (Kirk et al. 2016).

Six of the stars in our sample were already known as EBs and we confirm this classification using the *TESS* data: HD 6882 (ζ Phe), HD 61644 (V455 Car), HD 224113 (AL Scl), HD 42933 (δ Pic), HD 31407 (AN Dor), and HD 46792 (AE Pic). Their light curves in Appendix B are of unprecedented quality and future modeling will improve their mass determinations. One of these stars (HD 42933) is known to have β Cep type pulsations detected from BRIght Target Explorer (BRITE) photometry (Pigulski et al. 2017). We confirm this variability. In addition, 3 objects (HD 224990, HD 269382, and HD 53921) were known spectroscopic binaries, while 10 more (HD 269676, HD 68520, HD 19400, HD 53921, HD 2884, HD 46860, HD 208433, HD 37854, HD 209014, and CPD-60 944) were listed as double or multiple stars in SIMBAD; the *TESS* light curves of these 13 non-EBs did not show traces of the binary nature. The only exception is HD 208433, which shows a single transit. In addition, we find four showing either ellipsoidal variation or rotational modulation: HD 268798, HD 222847, HD 20784 and HD 37935. None of these four stars have previously been identified as binaries, but HD37935 is a known Be star.

HD 53921 is a known spectroscopic magnetic binary, which was identified as a slowly pulsating B (SPB) star by De Cat & Aerts (2002). From the high-quality *TESS* light curves we find that the dominant frequency of 0.6054 day^{-1} shows a second harmonic. Based on this, as well as the morphology of the light curve, we deduce that this frequency is caused by rotational modulation. This example illustrates how difficult g-mode asteroseismology from ground-based observations can be. This and other known magnetic stars in the sample are discussed in detail in A. David-Uraz et al. (2019, in preparation).

In total, 8 of these 19 binaries reveal pulsations. We show the phased light curve for a newly discovered binary pulsator (HD 61644 = TIC 349907707) in Figure 2. This result illustrates

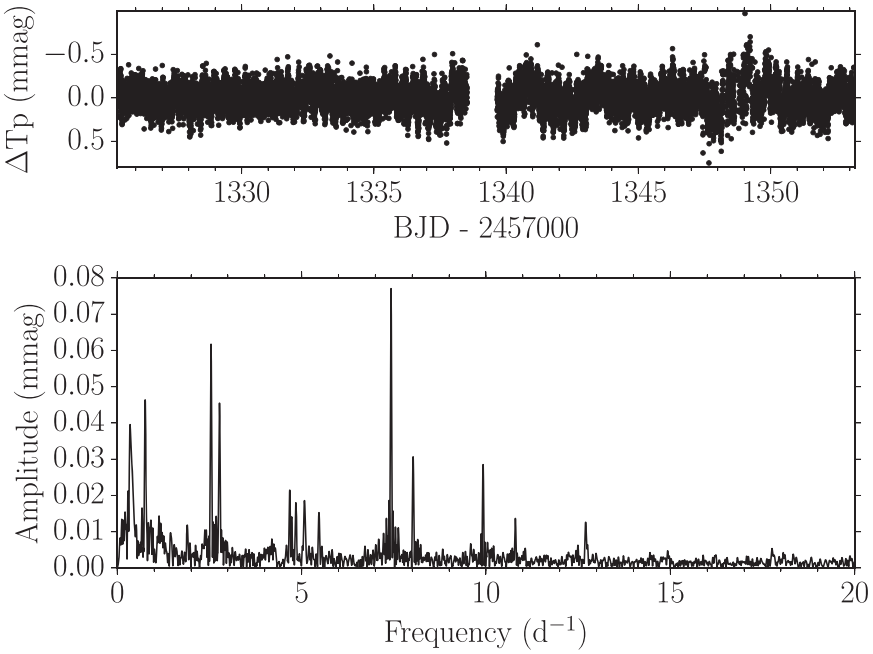

Figure 3. Example of a newly discovered hybrid pulsator showing both SPB and β Cep type pulsations (TIC 469906369 = HD 212581). The *TESS* light curve and amplitude spectrum are shown in the top and bottom panels, respectively.

the promise of *TESS* to provide numerous pulsating O and B binaries suitable to calibrate stellar evolution models from binary asteroseismology (Johnston et al. 2019).

3.2. Pulsating Stars

Coherent non-radial oscillation modes in O and B stars come in two main flavors: pressure modes with periods of a few hours (β Cepstars, spectral types from O9 to B3) and gravity modes with periods of order a few days (SPB stars, spectral types from late O to B9). For a discussion on their early discoveries and pulsation properties, we refer to Aerts et al. (2010, Chapter 2). The space-based photometry assembled with *MOST*, *CoRoT*, *Kepler*, *K2*, and BRITE revealed that many O and B pulsators are *hybrids*, i.e., pulsators with both types of modes simultaneously. Such hybrid pulsators have proven to be a powerful tool for constraining opacities in the partial ionization layers responsible for the mode excitation. As an example, the detailed seismic modeling of ν Eri performed by Daszyńska-Daszkiewicz et al. (2017) revealed that a factor three increase in the opacity at log $T = 5.46$ was needed to excite the g-modes in this star.

In total, we find 14 new O and B pulsators, among which 10 have gravity modes and 4 are potential hybrids. We show the light curve and DFT for one of the newly discovered hybrid stars in Figure 3. One star in the sample, HN Aqr, is a known β Cep star and is discussed in Handler et al. (2019). Future continued *TESS* and/or spectroscopic monitoring will be needed to assess the asteroseismic potential of these 14 pulsators in terms of frequency precision and mode identification.

3.3. Rotational Variability

We classified 21 of the stars in our sample as rotational variables, one of which is labeled as a Wolf–Rayet star in SIMBAD (HD 269582). Among these are three stars previously known to be magnetic: HD 223640 (Bychkov et al. 2005; Sikora et al. 2019) and HD 53921 (Hubrig et al. 2006; Bagnulo et al. 2015), as well as HD 65987 (Bagnulo et al. 2015). Rotational modulation is usually interpreted as being due to temperature and/or chemical spots on the stellar surface caused by large-scale magnetic fields. We refer to the accompanying papers by A. David-Uraz et al. (2019, in preparation) and Balona et al. (2019) for an extensive discussion of the rotational modulation and magnetic properties of the sample.

The star HD 10144 (also known as Achernar and α Eri) is a Be star rotating at 95% of critical breakup, whose stellar disk has been imaged by interferometry (Dalla Vedova et al. 2017). We find its dominant frequency to be 0.729 day^{-1}. Also HD 214748, HD 209522, HD 33599, HD 19818, HD 221507, HD 46860, HD 37974, HD 53048, CD-56 152, HD 209014, HD 37935, HD 68423, HD 224686, and HD 66194 were known to be Be stars prior to our study. While HD 221507 is known as a Be star, recent studies have shown that it lacks emission and has a low v sin i (e.g., Arcos et al. 2017).

In addition to the stars classified as rotational variables, we found 25 stars that show rotational modulation and/or SPB type variability. The simultaneous occurrence of rotation and pulsation frequencies in space photometry is not unusual, but there is only one case so far for which combined spectropolarimetric and asteroseismic modeling has been achieved: the hybrid magnetic β Cep/SPB star HD 43317 monitored by *CoRoT* (Buysschaert et al. 2017a, 2018). Our results are encourage expanding the domain of magneto-asteroseismology.

3.4. Stochastic, Low-frequency (SLF) Signatures

SLF variability has been shown to be a common phenomenon in blue supergiants in both space-based photometry (Bowman et al. 2019a) and spectroscopy (Simón-Díaz et al. 2018). Several theories may explain this variability, such as subsurface convection, dynamical stellar winds, and IGWs excited at the convective core boundary (see Bowman et al. 2019a, for a detailed discussion). In

our sample of 154 O and B stars, we find 25 stars with SLF, all of which are classified as blue supergiants based on the spectral types from SIMBAD and occurring near the terminal age main sequence (TAMS). This is in agreement with the conclusions by Bowman et al. (2019b) from *K2* photometry of such stars, and opens up an entirely new avenue of forward modeling of evolved OB stars at and beyond the TAMS to tune their angular momentum and element transport observationally.

3.5. Other Types of Variability

We found several stars with "outbursts" in their light curves (see Table 1 and Appendix B). Such outbursts may be connected with episodic mass loss, such as in Be stars, or flaring due to magnetic activity in low-mass stars. In some cases, the detected outbursts occur in various of the light curves at the same time and for the same duration. This signature is instrumental. For the remainder of the targets, spectroscopic follow-up and a study of the pixel data is required to confirm that the outbursts are physical, rather than instrumental artefacts (Pedersen et al. 2017, Balona et al. 2019).

4. Discussion and Conclusions

We presented variability classification for 154 stars with spectral type O or B that were monitored in short-cadence (2 minutes) by the *TESS* mission in its Sectors 1 and 2. We found 138 to be variable at the *TESS* detection threshold. This is a high percentage of variability (90%) given that the time base of each sector is only 27 days, preventing longer-period variables from being discovered. We placed the 151 out of 154 targets with a *Gaia* DR2 parallax in a CMD (Figure 1).

Our variability classification had the main goal to start compiling a large unbiased sample of O and B stars for future asteroseismology. Stars with multiple individual frequencies of identified coherent standing modes and/or low-frequency stochastically excited IGWs are suitable of asteroseismic probing. We found 15 single and 8 binary O and B coherent pulsators (i.e., 15% of the monitored stars) and 25 stars with stochastic low-frequency signatures (16%). All of these 25 stars are located in the LMC and cover a higher mass regime than the galactic targets. Unlike coherent modes, IGW driven by the convective core are independent of an iron opacity bump and should thus also be excited in low-metallicity stars. However, the low-frequency signal could also be produced by subsurface convection, which is strongly metal dependent (Cantiello et al. 2009). For all of the variable OB stars, an extension of the *TESS* light curve monitoring is needed to provide the frequency precision required for detailed asteroseismic modeling. Our initial study reveals the major potential of the combined long-term (+1 yr) *TESS*, Gaia, and spectroscopic all-sky monitoring as already outlined by Kollmeier et al. (2017).

This Letter includes data collected by the *TESS* mission. Funding for the *TESS* mission is provided by the NASA Explorer Program. Funding for the *TESS* Asteroseismic Science Operations Centre is provided by the Danish National Research Foundation (grant agreement No. DNRF106), ESA PRODEX (PEA 4000119301) and Stellar Astrophysics Centre (SAC) at Aarhus University. We thank the *TESS* and TASC/TASOC teams for their support of the present work. This research has made use of the SIMBAD database, operated at CDS, Strasbourg, France. Some of the data presented in this Letter were obtained from the Mikulski Archive for Space Telescopes (MAST). STScI is operated by the Association of Universities for Research in Astronomy, Inc., under NASA contract NAS5-2655. We acknowledge the ESO Science Archive Facility. The research leading to these results received funding and/or support from: the European Research Council (ERC) under the European Union's Horizon 2020 research and innovation program (grant agreement No. 670519: MAMSIE), the Research Foundation Flanders (FWO) under the grant agreement No. G0H5416N (ERC runner-up grant), the STFC consolidated grant No. ST/R000603/1, the Polish NCN grant (No. 2015/17/B/ST9/02082, 2015/18/A/ST9/00578 ,and 2016/21/B/ST9/01126), and the Natural Science and Engineering Research Council (NSERC) of Canada. The Flatiron Institute is supported by the Simons Foundation.

Appendix A
Variability Classification

In Table 1, we provide the *TESS* Input Catalogue (TIC) and *Gaia* identification numbers, as well as *Gaia* magnitudes and colors, SIMBAD spectral types, and the classification of the dominant source(s) of variability for each of the 154 O and B stars observed by *TESS* in sectors 1 and 2 at a 2 minutes cadence.

Table 1
Identification Numbers, Parameters, and Variability Classification of the 154 O and B Stars

TIC	Name	Sp. Type SIMBAD	Gaia DR2 ID	M_G (mag)	BP–RP (mag)	# Spectra	Instrument	Var. Type
12359289	HD 225119	Apsi	2333119869770412288	−0.98	−0.12	1	F	rot
29990592	HD 268623	B2Ia	4657589254497529344	−4.10	0.07	1	F	SLF
30110048	HD 268653	B3Ia	4765410903770283008	−2.02	−0.22	1	F	SLF
30268695	HD 268809	B1Ia	5290767631226220032	−2.20	−0.10	1	F	SLF
30275662	Sk-66 27	B3Ia	4661771801060664064	−3.37	−0.04	4	U	SLF
30275861	[HT83] alf	O6V	4662155839823561216	1.47	−0.13	⋯	⋯	rot
30312676	HD 268726	B2Ia	4662153812635167488	−2.87	0.01	2	U	SLF
30312711	BI 42	O8V	⋯	⋯	⋯	⋯	⋯	SLF/rot/EB?
30317301	HD 268798	B2Ia	4661511422956353152	−3.02	0.00	⋯	⋯	EV/rot/SLF
30933383	Sk-68 39	B2.5Ia	4662153469001983104	−2.97	0.12	2	F	SLF
31105740	TYC 9161-925-1	B0.5Ia	4655458160445111552	−2.93	−0.15	1/3	F/U	SLF
31181554	HD 269050	B0Ia	4661392533937464448	−2.05	−0.22	22/12	X/U	SLF
31867144	HD 22252	B8IV	4671120982756449664	−1.11	−0.01	⋯	⋯	rot/SPB + β Cephybrid?
33945685	HD 223118	B9.5V	2338752697903817216	1.29	0.04	⋯	⋯	instr? ($\nu_{\rm inst} \simeq 2.8$ day^{-1})/puls
38602305	HD 27657 AB	B9IV	4676067719930656640	0.28	−0.11	⋯	⋯	rot
40343782	HD 269101	B3Iab	5288240197589081728	−3.18	0.04	⋯	⋯	SLF/SPB?
41331819	HD 43107	B8V	5282761464287879296	0.29	−0.09	84/12	X/U	rot/outburst?
47296054	HD 214748	B8Ve	6622561673163632768	−1.38	−0.10	26	U	rot/SPB/Be
49687057	HD 220787	B3III	4657674745869490304	−2.38	0.15	6/18	F/X	instr/binary?
53992511	HD 209522	B4IVe	2436569757731466112	−2.04	−0.25	3/18/1/15	F/X/E/U	rot/SPB/Be
55295028	HD 33599	B2Vpe	6619440159652409728	−1.60	−0.23	1	F	rot/SPB/Be
66497441	HD 222847	B9V	2391220091406075648	−0.10	−0.08	1/42	F/U	EV/rot?/SPB?
69925250	V* HN Aqr	B	2402031280004432512	−1.58	−0.30	4	U	known β Cep
89545031	HD 223640	A0VpSiSr	2390144081839340288	0.10	−0.15	33	U	rot
92136299	HD 222661 A	B9V	2419885149815948416	0.99	−0.06	28	U	SPB+Be-type mini-outbursts/rot
115177591	HD 201108	B8IV/V	6775980889978989824	−0.16	−0.07	⋯	⋯	SPB
139468902	HD 213155	B9.5V	6521195703338406272	1.01	−0.05	1/63/1	F/X/U	rot/SPB?
141281495	HD 37854	B9/9.5V	4648666996817764736	0.57	−0.02	⋯	⋯	rot?
149039372	HD 34543	B8V	4663645952980782848	0.30	−0.05	⋯	⋯	rot?/SPB?
149971754	HD 41297	B8Ib	5482011113182765696	−0.26	−0.11	⋯	⋯	SPB
150357404	HD 45796	B6V	5477233430220256384	−0.44	−0.17	1	F	SPB
150442264	HD 46792	B2V	4760693797025929344	−3.24	−0.21	⋯	⋯	EB + puls/rot
152283270	HD 208433	B9.5V	6588214059487740672	0.25	−0.01	⋯	⋯	instr/binary(transit)
167045028	HD 45527	B9IV	5279546835885790720	0.01	−0.03	⋯	⋯	rot
167415960	HD 48467	B8/9V	5266733784509615616	0.11	−0.08	1	F	const?
167523976	HD 49193	B2V	4660166788974686976	−1.48	−0.22	⋯	⋯	SPB
176935619	HD 49306	B9.5/A0V	5280155179351701504	1.02	−0.05	⋯	⋯	instr? ($\nu_{\rm inst} \simeq 2.8$ day^{-1})
176955379	HD 49531	B8/9Vn	5279020208473101056	0.45	−0.04	⋯	⋯	SPB/rot
177075997	HD 51557	B7III	5266581089830743296	−0.99	−0.15	1	F	instr/rot?
179308923	HD 269382	O9.5Ib	4657651857940816640	−2.57	−0.05	⋯	⋯	SLF?/SPB?
179574710	HD 271213	B1Iak	4661778810447390720	−1.47	−0.09	⋯	⋯	SLF
179637387	[OM95] LH 47-373A	B1Ia	4651354886129065600	−1.52	−0.10	⋯	⋯	SLF
179639066	HD 269440	B1Ib	4658741370886084992	−2.17	−0.10	2	F	SLF
182909257	HD 6783	Ap Si	4635279171434162304	0.65	−0.04	⋯	⋯	rot
197641601	HD 207971	B8IV-Vs	6586825380598277248	−1.97	2.13	22	U	instr/rot
206362352	HD 223145	B3V	5283754052709233920	−2.30	−0.22	1/3/302	F/X/U	SPB

Table 1
(Continued)

TIC	Name	Sp. Type SIMBAD	Gaia DR2 ID	M_G (mag)	BP–RP (mag)	# Spectra	Instrument	Var. Type
206547467	HD 210780	B9.5/A0	6819470079550296960	1.74	0.07	⋯	⋯	rot/const?/SPB?
207176480	HD 19818	B9/A0Vn(e)	4723685987980665088	1.59	0.25	3	F	SPB?/SLF?/Be
207235278	HD 20784	B9.5V	4733510055655723392	−0.98	0.01	⋯	⋯	EV/rot
220430912	HD 31407	B2/3V	6522301330997312128	−1.06	−0.25	84	X	EB + puls
224244458	HD 221507	B9.5IIIpHgMnSi	6538585991555664128	0.59	−0.12	3/30	F/U	rot + mini-outburst?
229013861	HD 208674	B9.5V	6612822091790516480	1.07	−0.04	⋯	⋯	rot
230981971	HD 10144	B6Vpe	⋯	⋯	⋯	217/270	F/U	rot/SPB?/Be
231122278	HD 29994	B8/9V	4656238611846958208	0.53	0.04	⋯	⋯	rot/SPB?
238194921	HD 24579	B7III	4627113682690040576	−0.35	−0.04	⋯	⋯	rot/SPB
259862349	HD 16978	B9Va	4695167130257150592	0.66	−0.07	6/9/20	F/X/U	instr
260128701	HD 42918	B4V	5494534348761557888	−1.01	−0.25	⋯	⋯	SPB
260131665	HD 42933	B1/2(III)n	5499415974230271488	−3.45	−0.36	4	F	EB + β Cep
260368525	HD 44937	B9.5V	5494983804202264192	−0.18	0.11	⋯	⋯	SPB?
260540898	HD 46212	B8IV	5496276314480471040	−0.55	−0.02	⋯	⋯	rot?
260640910	HD 46860 AB	B9IVn+A8V:p?	5482771807727582080	−0.73	−0.08	2	F	SPB/Be
260820871	HD 218801	B9.5V(n)	6381543153782126464	0.60	−0.05	⋯	⋯	rot/binary?
261205462	HD 40953	B9V	4623532264081294464	0.66	−0.08	1	F	SPB/rot
262815962	HD 218976 AB	B9.5/A0V	6500025053617700992	1.32	−0.01	⋯	⋯	rot/SPB?
270070443	HD 198174	B8II	6805364208656989696	−0.31	−0.08	⋯	⋯	rot
270219259	HD 209014 AB	B8/9V+B8/9	6617682865193265536	−1.40	0.23	3	F	instr/β Cep+ outburst
270557257	HD 49835	B9.5V	5211969859107211136	1.40	0.14	⋯	⋯	instr ($\nu_{\rm inst} \simeq 2.8$ day^{-1})
270622440	HD 224112	B8V	2314214110928211712	−0.08	−0.10	3	F	EB (contamination!)
270622446	HD 224113	B5/8	2314213698611350144	−0.78	−0.12	36/18	F/X	EB
271503441	HD 2884 AB	B8/A0	4900927434176620160	1.12	−0.08	11	F	SPB?/outburst?
271971626	HD 62153 AB	B9IV	5214590201474858624	−0.01	−0.01	⋯	⋯	rot
276864600	HD 269777	B3Ia	4661270350708775296	−1.90	−0.05	5	F	SLF
277022505	HD 269786	B1I	4657274283151403520	−3.66	−0.00	⋯	⋯	SLF
277022967	HD 37836	B0e(q)	4657280639705552768	−4.54	0.34	12/70	F/X	rot/SPB?/ SLF?/ Be
277099925	HD 269845	B2.5Ia	4661439439319405184	−2.67	−0.04	⋯	⋯	SLF
277103567	HD 37935	B9.5V	4660284883361750912	−0.48	−0.04	2/30	F/X	rot/EV?
277172980	HD 37974	B0.5e	4657658356271368064	−4.36	0.51	11/6	F/X	SLF?/Be
277173650	HD 269859	B1Ia	4658882353222625920	−3.23	−0.16	40	X	SLF/instr?
277298891	Sk-69 237	B1Ia	4657679659311713024	−1.39	0.39	1	F	SLF
277982164	HD 54239	B9.5/A0III/IV	5211241295215037696	−0.01	0.16	36	U	rot/SPB
278683664	HD 47770	B9.5V	5484286625513030016	0.76	0.04	⋯	⋯	const??
278865766	HD 48971	B9V	5496814662861807360	0.46	−0.02	⋯	⋯	const??
278867172	HD 49111	B9.5V	5497973449334379904	0.96	−0.04	⋯	⋯	const??
279430029	HD 53048	B5/7Vn(e)	5484134029618653952	−1.97	−0.02	⋯	⋯	rot/Be
279511712	HD 53921 AB	B9III+B8V	5480486644608749696	−0.12	−0.17	⋯	⋯	rot
279957111	HD 269582	WN10h	4658481718680657792	−3.51	0.33	211	X	rot
280051467	HD 19400 AB	B8III/IV	4645479443883933824	−0.45	−0.16	1/238	F/U	rot
280684074	HD 215573	B6V	6351882320090933248	−0.70	−0.19	1/8	F/U	SPB
281703963	HD 4150 A	A0IV	4908022136034353152	−0.12	0.02	1	F	hybrid SPB/δ Sct
281741629	CD-56 152	Be	4908668373993964032	−3.05	−0.23	2/6	F/U	rot/Be
293268667	HD 47478	B9V	5477090356269215616	0.60	−0.08	⋯	⋯	SPB/rot?

Table 1
(Continued)

TIC	Name	Sp. Type SIMBAD	Gaia DR2 ID	M_G (mag)	BP–RP (mag)	# Spectra	Instrument	Var. Type
293973218	HD 54967	B4V	5478303942228108288	−2.08	−0.21	⋯	⋯	rot/SPB
294747615	HD 30612	B8II/III(pSi)	4654833539071572736	−0.33	−0.15	1	F	rot/SLF?
294872353	HD 270754	B1.5Ia	4657655435693905408	−4.36	−0.02	1/20	F/U	SLF?
300010961	HD 55478	B8III	5280667689208638976	−0.00	−0.14	⋯	⋯	rot/β Cep?
300325379	HD 58916	B1.5Ia	5281254278662916736	0.41	0.01	⋯	⋯	rot?
300329728	HD 59426	B9V	5267524573886888320	0.72	0.05	⋯	⋯	rot
300744369	HD 63928	B9V	5270696836731782144	1.08	0.01	⋯	⋯	rot
300865934	HD 64484	B9V	5275049837626917504	0.04	−0.06	⋯	⋯	instr/outburst?
306672432	HD 67252	B8/9V	5271283391825477248	0.76	−0.01	⋯	⋯	const?/rot?
306824672	HD 68221	B9V	5270992635422817792	0.05	0.04	⋯	⋯	rot?/SPB?
306829961	HD 68520 AB	B5III	5270986008289935232	−2.44	−0.15	⋯	⋯	SPB
307291308	HD 71066	B9/A0IV	5221286296008492416	0.06	−0.13	13	U	instr/rot?
307291318	HD 71046 AB	B9III/IV	5221286158569529344	−0.17	−0.09	⋯	⋯	instr/rot?
307993483	HD 73990	B7/8V	5221605085661325056	0.40	−0.07	⋯	⋯	β Cep?/SPB
308395911	HD 66591	B4V	5479669466951012224	−1.33	−0.15	2	F	SPB
308454245	HD 67420	B9V	5275660856854591360	0.39	0.07	⋯	⋯	δ Sct
308456810	HD 67170	B8III/IV	5289613208437434240	0.05	0.04	⋯	⋯	rot?
308537791	HD 67277	B8III	5290024533163062144	0.18	−0.01	⋯	⋯	rot
308748912	HD 68423	B6V	5277219758184463488	−0.74	−0.06	⋯	⋯	SLF?/outburst?/instr
309702035	HD 271163	B3Ia	4660142634076536320	−3.61	−0.03	⋯	⋯	SLF
313934087	HD 224990	B3/5V	2320885329010329216	−1.32	−0.19	4/18	F/X	SPB/rot
327856894	HD 225253	B8IV/V	4701860922688030720	−0.80	−0.14	3/109	F/U	rot?/outburst?/ instr?
349829477	HD 61267	B9/A0IV	5292390815325246976	1.07	0.09	⋯	⋯	const?
349907707	HD 61644	B5/6IV	5289291395127135360	−0.35	0.23	⋯	⋯	EB + puls
350146577	HD 63204	ApSi	5288156497263051136	0.65	−0.03	⋯	⋯	rot
350823719	HD 41037	B3V	5275962500997316864	−0.88	−0.23	5/6	F/U	SPB?/rot
354671857	HD 14228	B8IV	4936685751335824896	0.15	3.16	10/79	F/U	SPB?/rot
355141264	HD 208495	B9.5V	6561093750492347136	1.30	−0.03	⋯	⋯	const?
355477670	HD 220802	B9V	6525840590207613824	0.34	−0.09	8	F	const?
355653322	HD 224686	B8V	6485326438580933888	−0.74	−0.07	52	F	rot?/outburst?/instr?
358232450	HD 6882 A	B6V+B9V	4913847589156808960	0.10	−0.18	24/33	F/U	EB
358466708	CD-60 1931	B7	5290739387520374912	−0.04	−0.01	⋯	⋯	rot/SPB
358467049	CPD-60 944 AB	B8pSi	5290722929205920640	0.18	0.06	⋯	⋯	rot
358467087	CD-60 1929	B8.5IV	5290722860486442752	0.36	0.13	⋯	⋯	SPB/EV?/rot? /SLF?/ instr?
364323837	HD 40031	B6III	4758153203612698624	−1.44	−0.13	4	F	rot?/SPB?
364398190	CD-60 1978	B8.5IV-V	5290816009737675392	0.64	0.05	⋯	⋯	rot?/SLF?
364398342	HD 66194	B3Vn	4776318613169946624	−2.36	−0.33	97	U	rot?/SPB?/Be
364421326	HD 66109	B9.5V	5287999576341359360	−0.18	0.08	⋯	⋯	rot?
369457005	HD 197630	B8/9V	6681797793393053696	0.44	−0.11	1/15	F/U	rot/SPB?
370038084	HD 26109	B9.5/A0V	4666380781970681472	1.65	0.19	⋯	⋯	const?
372913233	HD 65950	B8III	5290671733195996416	−1.20	0.06	5	F	const?/outburst?/instr?
372913582	CD-60 1954	B9.5V	5290725643625189504	0.29	0.11	⋯	⋯	const?/outburst?/instr?
372913684	HD 65987	B9.5IVpSi	5290820682661822848	−0.67	−0.02	⋯	⋯	rot
373843852	HD 269525	B0I	4658678973606061696	−2.39	−0.32	⋯	⋯	SPB?/rot?
389921913	HD 270196	B1.5Ia	4662413606586588160	−2.83	0.09	1/8	F/U	SLF

Table 1
(Continued)

TIC	Name	Sp. Type SIMBAD	Gaia DR2 ID	M_G (mag)	BP–RP (mag)	# Spectra	Instrument	Var. Type
391810734	HD 269655	B0Ia	4661289630893455488	−2.51	−0.11	2	F	SLF
391887875	HD 269660	B2Ia	4657362548954664192	−3.36	−0.14	⋯	⋯	SLF
404768847	VFTS 533	B0Ia	4651835308326981504	−1.95	−0.06	⋯	⋯	SPB?/SLF?
404768956	Cl* NGC 2070 Mel 12	B0.5Ia	4658479691454645504	−2.91	0.03	⋯	⋯	SLF?/SPB?/instr?
404796860	HD 269920	B3Ia	4657652476416109184	−3.84	0.04	⋯	⋯	SLF
404852071	Sk-69 265	B3I	4660612881443486720	−2.93	−0.09	⋯	⋯	SLF
404933493	HD 269997	B2.5Ia	4660135826507549824	−3.14	−0.06	1	F	SLF
404967301	HD 269992	B2.5Ia	4657636675267019008	−3.51	0.18	2	F	SLF
410447919	HD 64811	B4III	⋯	⋯	⋯	⋯	⋯	rot/SPB?
410451677	HD 66409	B8IV/V	5290769211774211968	0.32	0.05	4	F	rot
419065817	HD 1256	B6III/IV	2364986843479227392	0.13	−0.13	⋯	⋯	rot/SPB?
425057879	HD 269676	O6+O9	4651834616802932608	−1.79	−0.20	⋯	⋯	instr?/binary?/rot?
425081475	HD 269700	B1.5Iaeq	4657685534828270976	−2.78	0.33	1/48	F/X	SLF/rot?/Be
425083410	HD 269698	O4Ia	4660121743354291328	−2.38	−0.34	6	U	rot/SPB?/SLF?
425084841	TYC 8891-3638-1	B1Ia	4658474743652257664	−3.93	0.04	2/6	F/U	SLF
441182258	HD 210934	B7V	6618669608159645312	−0.53	−0.14	⋯	⋯	instr/SPB/outburst?
441196602	HD 211993	B8/9V	6615398767225726848	0.46	−0.09	2/9	U/X	const?
469906369	HD 212581 AB	B9Vn+G0V	6404338508023617664	−0.10	−0.03	19	U	SPB/β Cep/instrumental?

Note. EB = eclipsing binary; EV = ellipsoidal variable; rot = Rotational modulation; SPB; β Cep; SLF = stochastic low-frequency signal; instr = instrumental; const = constant; puls = pulsational signal not clearly identified in any of the previous categories; and δ Sct = δ Scuti star. We provide and overview of which stars have high-resolution spectra available in the ESO archive. U = UVES; F = FEROS; X = X-SHOOTER; E = ESPRESSO. Stars with TIC numbers in *italics* are LMC members.

(This table is available in machine-readable form.)

Appendix B
TESS Light Curves and Amplitude Spectra

The light curves and amplitude spectra for the 154 O and B stars considered in this work are shown in Figure 4.

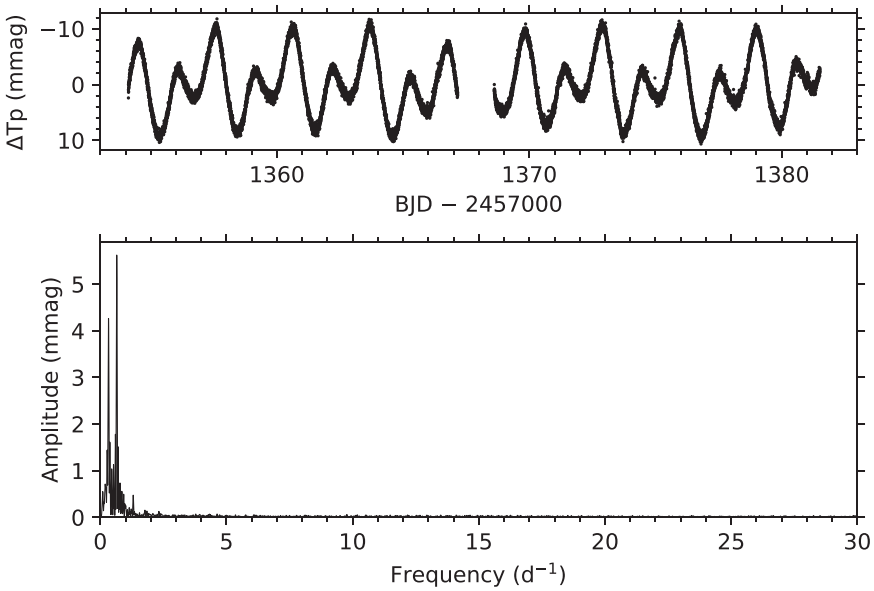

Figure 4. *TESS* light curve (top) and amplitude spectrum (bottom) of TIC 12359289. The complete figure set (154 images) for all stars considered in this Letter is available in the online journal.

(The complete figure set (154 images) is available.)

ORCID iDs

May G. Pedersen https://orcid.org/0000-0002-7950-0061
Sowgata Chowdhury https://orcid.org/0000-0001-7444-5131
Cole Johnston https://orcid.org/0000-0002-3054-4135
Dominic M. Bowman https://orcid.org/0000-0001-7402-3852
Conny Aerts https://orcid.org/0000-0003-1822-7126
Gerald Handler https://orcid.org/0000-0001-7756-1568
Peter De Cat https://orcid.org/0000-0001-5419-2042
Coralie Neiner https://orcid.org/0000-0003-1978-9809
Alexandre David-Uraz https://orcid.org/0000-0003-4062-0776
Derek Buzasi https://orcid.org/0000-0002-1988-143X
Andrew Tkachenko https://orcid.org/0000-0003-0842-2374
Sergio Simón-Díaz https://orcid.org/0000-0003-1168-3524
Ehsan Moravveji https://orcid.org/0000-0003-4372-0588
James Sikora https://orcid.org/0000-0002-3522-5846
Giovanni M. Mirouh https://orcid.org/0000-0003-0238-8435
Catherine C. Lovekin https://orcid.org/0000-0003-4233-3105
Matteo Cantiello https://orcid.org/0000-0002-8171-8596
Jadwiga Daszyńska-Daszkiewicz https://orcid.org/0000-0001-9704-6408
Andrzej Pigulski https://orcid.org/0000-0003-2488-6726
Roland K. Vanderspek https://orcid.org/0000-0001-6763-6562
George R. Ricker https://orcid.org/0000-0003-2058-6662

References

Aerts, C. 2015, in IAU Symp. 307, New Windows on Massive Stars, ed. G. Meynet et al. (Cambridge: Cambridge Univ. Press), 154
Aerts, C., Bowman, D. M., Símon-Díaz, S., et al. 2018a, MNRAS, 476, 1234
Aerts, C., Christensen-Dalsgaard, J., & Kurtz, D. W. 2010, Asteroseismology (Heidelberg: Springer)
Aerts, C., Mathis, S., & Rogers, T. 2019, ARA&A, in press (arXiv:1809.07779)
Aerts, C., Molenberghs, G., Michielsen, M., et al. 2018b, ApJS, 237, 15
Aerts, C., & Rogers, T. M. 2015, ApJL, 806, L33
Almeida, L. A., Sana, H., Taylor, W., et al. 2017, A&A, 598, A84
Arcos, C., Jones, C. E., Sigut, T. A. A., Kanaan, S., & Curé, M. 2017, ApJ, 842, 48
Bagnulo, S., Fossati, L., Landstreet, J. D., & Izzo, C. 2015, A&A, 583, A115
Bailer-Jones, C. A. L., Rybizki, J., Fouesneau, M., Mantelet, G., & Andrae, R. 2018, AJ, 156, 58
Balona, L. A., Handler, G., Chowdhury, S., et al. 2019, MNRAS, submitted
Bowman, D. M. 2017, Amplitude Modulation of Pulsation Modes in Delta Scuti Stars (Cham: Springer)
Bowman, D. M., Aerts, C., Johnston, C., et al. 2019a, A&A, 621, A135
Bowman, D. M., Burssens, S., Pedersen, M. G., et al. 2019b, NatAs, submitted
Buysschaert, B., Aerts, C., Bloemen, S., et al. 2015, MNRAS, 453, 89
Buysschaert, B., Aerts, C., Bowman, D. M., et al. 2018, A&A, 616, A148
Buysschaert, B., Neiner, C., Briquet, M., & Aerts, C. 2017a, A&A, 605, A104
Buysschaert, B., Neiner, C., Richardson, N. D., et al. 2017b, A&A, 602, A91
Bychkov, V. D., Bychkova, L. V., & Madej, J. 2005, A&A, 430, 1143
Cantiello, M., Langer, N., Brott, I., et al. 2009, A&A, 499, 279
Castor, J. I., Abbott, D. C., & Klein, R. I. 1975, ApJ, 195, 157
Dalla Vedova, G., Millour, F., Domiciano de Souza, A., et al. 2017, A&A, 601, A118
Daszyńska-Daszkiewicz, J., Pamyatnykh, A. A., Walczak, P., et al. 2017, MNRAS, 466, 2284
De Cat, P., & Aerts, C. 2002, A&A, 393, 965
Gaia Collaboration, Brown, A. G. A., Vallenari, A., et al. 2018a, A&A, 616, A1
Gaia Collaboration, Eyer, L., Rimoldini, L., et al. 2018b, A&A, in press (arXiv:1804.09382)
Hubrig, S., North, P., Schöller, M., & Mathys, G. 2006, AN, 327, 289
Handler, G., Andrzej, P., Daszyńska-Daszkiewicz, J., et al. 2019, ApJL, submitted
Johnston, C., Buysschaert, B., Tkachenko, A., Aerts, C., & Neiner, C. 2017, MNRAS, 469, L118
Johnston, C., Tkachenko, A., Aerts, C., et al. 2019, MNRAS, 482, 1231
Kallinger, T., Weiss, W. W., Beck, P. G., et al. 2017, A&A, 603, A13

Kirk, B., Conroy, K., Prša, A., et al. 2016, AJ, 151, 68
Kollmeier, J. A., Zasowski, G., Rix, H.-W., et al. 2017, SDSS-V White Paper, arXiv:1711.03234
Krtička, J., & Feldmeier, A. 2018, A&A, 617, A121
Kurtz, D. W. 1985, MNRAS, 213, 773
Lucy, L. B., & Solomon, P. M. 1970, ApJ, 159, 879
Mombarg, J. S. G., Van Reeth, T., Pedersen, M. G., et al. 2019, MNRAS, submitted
Moravveji, E., Aerts, C., Pápics, P. I., Triana, S. A., & Vandoren, B. 2015, A&A, 580, A27
Moravveji, E., Townsend, R. H. D., Aerts, C., & Mathis, S. 2016, ApJ, 823, 130
Owocki, S. P., & Rybicki, G. B. 1984, ApJ, 284, 337
Pablo, H., Richardson, N. D., Fuller, J., et al. 2017, MNRAS, 467, 2494
Pedersen, M. G., Antoci, V., Korhonen, H., et al. 2017, MNRAS, 466, 3060
Pigulski, A., Jerzykiewicz, M., Ratajczak, M., Michalska, G., & Zahajkiewicz, E. 2017, in Proc. Polish Astronomical Society 5, Second BRITE-Constellation Science Conf.: Small Satellites—Big Science, ed. K. Zwintz & E. Poretti (Bartycka: Polish Astronomical Society), 120
Ramiaramanantsoa, T., Moffat, A. F. J., Harmon, R., et al. 2018a, MNRAS, 473, 5532
Ramiaramanantsoa, T., Ratnasingam, R., Shenar, T., et al. 2018b, MNRAS, 480, 972
Ricker, G. R., Winn, J. N., Vanderspek, R., et al. 2015, JATIS, 1, 014003
Sana, H., Le Bouquin, J.-B., Lacour, S., et al. 2014, ApJS, 215, 15
Schneider, F. R. N., Sana, H., Evans, C. J., et al. 2018, Sci, 359, 69
Sikora, J., Wade, G. A., Power, J., & Neiner, C. 2019, MNRAS, 483, 3127
Simón-Díaz, S., Aerts, C., Urbaneja, M. A., et al. 2018, A&A, 612, A40
Szewczuk, W., & Daszyńska-Daszkiewicz, J. 2018, MNRAS, 478, 2243
Torres, G., Andersen, J., & Giménez, A. 2010, A&ARv, 18, 67